Surveys in Geophysics
https://doi.org/10.1007/s10712-024-09861-9

The Global Energy Balance as Represented in Atmospheric Reanalyses

Martin Wild[1] · **Michael G. Bosilovich**[2]

Received: 6 March 2024 / Accepted: 2 September 2024

Abstract
In this study, we investigate the representation of the global mean energy balance components in 10 atmospheric reanalyses, and compare their magnitudes with recent reference estimates as well as the ones simulated by the latest generation of climate models from the 6th phase of the coupled model intercomparison project (CMIP6). Despite the assimilation of comprehensive observational data in reanalyses, the spread amongst the magnitudes of their global energy balance components generally remains substantial, up to more than 20 Wm^{-2} in some quantities, and their consistency is typically not higher than amongst the much less observationally constrained CMIP6 models. Relative spreads are particularly large in the reanalysis global mean latent heat fluxes (exceeding 20%) and associated intensity of the global water cycle, as well as in the energy imbalances at the top-of-atmosphere and surface. A comparison of reanalysis runs in full assimilation mode with corresponding runs constrained only by sea surface temperatures reveals marginal differences in their global mean energy balance components. This indicates that discrepancies in the global energy balance components caused by the different model formulations amongst the reanalyses are hardly alleviated by the imposed observational constraints from the assimilation process. Similar to climate models, reanalyses overestimate the global mean surface downward shortwave radiation and underestimate the surface downward longwave radiation by 3–7 Wm^{-2}. While reanalyses are of tremendous value as references for many atmospheric parameters, they currently may not be suited to serve as references for the magnitudes of the global mean energy balance components.

Keywords Global energy balance · Reanalysis · Earth radiation budget · Surface energy balance · Earth's energy imbalance · Energy and water cycles

✉ Martin Wild
martin.wild@env.ethz.ch

[1] ETH Zurich, Institute for Atmospheric and Climate Science, 8092 Zurich, Switzerland

[2] Global Modeling and Assimilation Office, NASA Goddard Space Flight Center, Greenbelt, MD 20771, USA

Article Highlights

- The global mean energy balance components of 10 different reanalyses are compared to reference estimates and state-of-the-art climate models from CMIP6
- The spread in the global energy balance components amongst the reanalyses is substantial (exceeding 20 Wm^{-2} in some quantities) and typically not smaller than amongst the CMIP6 models
- The spread amongst the reanalyses is particularly large in global mean latent heat fluxes and associated intensity of the global water cycle, as well as in the representation of the Earth energy imbalance (EEI)
- Compared to reference estimates, the reanalyses tend to overestimate the global mean surface downward shortwave radiation, which is compensated by an underestimation of the surface downward longwave radiation

1 Introduction

The Earth's energy balance fundamentally determines the climatic conditions on our planet. While the energy balance at the top-of-atmosphere (TOA), consisting of the shortwave and longwave radiation fluxes in an out of the climate system, determines the overall heat uptake in the climate system, the energy balance at the surface governs the thermal changes in our environments and defines the radiative energy that drives the evaporative flux and with it the global water cycle (e.g., Kiehl and Trenberth 1997; Wild et al. 1998, 2013; Hatzianastassiou et al. 2004; Trenberth et al. 2009; Bosilovich et al. 2011; Stephens et al. 2012; Allan et al. 2014; L'Ecuyer et al. 2015; Hakuba et al. 2019; Wang et al. 2022). An accurate knowledge of the magnitude of these energy fluxes is therefore essential for an adequate quantification of the state of climate and climate change.

Atmospheric reanalyses are widely used as references for various climate parameters, as they assimilate comprehensive amounts of in situ and space-based weather observations from the Global Observing System (GOS) into a numerical model, which enables an observationally constrained representation of the three-dimensional atmospheric structure (e.g., Bosilovich et al. 2013). Reanalyses are thus much more constrained by observations than "free-running" climate models. While reanalyses provide well-accepted and widely used reference estimates for quantities like geopotential heights, sea level pressure or upper air temperature and humidity fields, their ability to adequately represent the global energy balance components is less comprehensively assessed. The representation of different global mean energy balance components in earlier and individual reanalyses have been evaluated by Allan et al. (2004) in the ERA-40 reanalysis, by Trenberth et al. (2009) in ERA-40 and early versions of the NCEP and JRA reanalyses, by Berrisford et al. (2011) in the ERA-Interim reanalysis, by Bosilovich et al. (2011) and (Roberts et al. 2012) in the MERRA reanalysis, and by Bosilovich et al. (2015) and (Stamatis et al. 2022) in the MERRA-2 reanalysis. Net surface energy fluxes using TOA radiation measurements combined with atmospheric energy transports and tendencies from reanalyses have been investigated by Trenberth and Solomon (1994) and Liu et al. (2017).

In the present study, we will focus in the following on the global energy balance as represented in 10 different reanalyses. We will cover all radiative energy balance components under both all-sky and clear-sky conditions, as well as the non-radiative surface energy balance components of sensible and latent heat. We will focus on the consistency in the magnitudes of these various energy balance components across the different reanalyses,

and compare them to independent reference estimates as well as to the respective quantities in state-of-the-art climate models participating in the 6th phase of the Coupled Model Intercomparison Project (CMIP6) as analyzed in Wild (2020).

2 Data

Data from 10 different reanalysis products are used in this study (Table 1). These include the reanalyses MERRA-2 (Gelaro et al. 2017), MERRA-2 AMIP (Collow et al. 2017) ERA5 (Hersbach et al. 2020), JRA-55 (Kobayashi et al. 2015), NCEP-R2 (Kanamitsu et al. 2002), 20CRv3 (Slivinski et al. 2019), ERA20C (Poli et al. 2016), ERA20CM (Hersbach et al. 2015), MERRA (Rienecker et al. 2011) and JRA-3Q (Kosaka et al. 2024). While MERRA, MERRA-2, ERA5, JRA-55, JRA-3Q and NCEP-R2 consider full data assimilation (i.e., as many observing platforms as the systems can assimilate including radiance assimilation), ERA20C and 20CRv3 only assimilate surface observations, whereas MERRA-2 AMIP as well as ERA20CM do not include any data assimilation except the evolution of sea surface temperatures and sea-ice extent, which is prescribed according to observations in all reanalysis products considered here. MERRA-2 AMIP as well as ERA20CM use identical physical models as their counterparts MERRA-2 and ERA20C, respectively. The only reanalysis that forces global mass conservation in the presence of water and/or dry mass assimilation is MERRA-2. Regionally, the water vapor and mass increments have significant magnitudes in the respective budgets (Takacs et al. 2016).

The values presented in this study are long-term global annual averages over the period 2001–2010, which is covered by all 10 reanalyses considered here. They are thus representative for the first decade of the twenty-first century. NCEP-R2 did not provide any clear-sky fluxes. While all other reanalyses provided net clear-sky shortwave and longwave radiation at the surface, none of them explicitly stored the related clear-sky downward components, which can be directly compared to surface observations. The clear-sky downward shortwave and longwave components were therefore inferred from the available quantities by combining the clear-sky surface net shortwave radiation with the surface albedo, and the clear-sky surface net longwave radiation with the upward longwave radiation, respectively.

With respect to reference estimates, we refer to published satellite-derived data from CERES-EBAF for the TOA and surface radiative components under all-sky and clear-sky conditions (Loeb et al. 2018; Kato et al. 2018), plus to independent estimates derived by Wild et al. (2015) and L'Ecuyer et al. (2015) for the all-sky radiative and non-radiative surface energy balance components, as well as to the clear-sky surface and atmospheric radiative estimates derived by Wild et al. (2019). Generally, global reference estimates of the TOA fluxes are afflicted with smaller uncertainties than their atmospheric and surface counterparts, since they can be directly measured from space, whereas the surface and atmospheric estimates must rely to some degree on modeling in addition to the available direct observations. Thus, the various surface and atmospheric energy balance estimates published over the years differed substantially. Their consistency has however improved in recent years, yet still not reaching the level of accuracy of the TOA estimates (Wild 2017).

In addition, the results of Wild (2020) covering the representation of the global mean energy balance components in up to 40 CMIP6 climate models are used for comparison. These stem from "historical-all-forcings" experiments and represent the global energy balance components as simulated in the CMIP6 models at the beginning of the twenty-first century.

Table 1 Global annual means of various energy balance components under clear-sky and all-sky conditions at the TOA, within the atmosphere and at the surface, representative for the first decade of the twenty-first century (2001–2010), as calculated in 10 individual reanalyses, together with reference estimates

Energy balance component	Reference Estimates Wm^{-2}	MERRA-2 Wm^{-2}	M2AMIP Wm^{-2}	ERA5 Wm^{-2}	JRA-55 Wm^{-2}	NCEP-R2 Wm^{-2}	20CRv3 Wm^{-2}	ERA20C Wm^{-2}	ERA20CM Wm^{-2}	MERRA Wm^{-2}	**JRA-3Q** Wm^{-2}
TOA											
SW down	340[a], 340[b], 340[c]	340.4	340.4	340.4	341.3	341.3	340.3	340.4	340.4	341.3	341.3
SW up all-sky	− 99[a], − 100[b], − 102[c]	− 106.0	− 104.2	− 97.6	− 100.0	− 104.8	− 98.2	− 100.5	− 99.2	− 99.5	− 96.8
SW absorbed all-sky	241[a], 240[b], 238[c]	234.4	236.2	242.8	241.3	236.5	242.1	239.9	241.2	241.8	244.6
SW up clear-sky	− 53[a], − 53[b]	− 51.4	− 51.1	− 51.4	− 55.3	DNR	− 57.4	− 51.2	− 51.4	− 52.3	− 51.2
SW absorbed clear-sky	287[a], 287[b]	289.0	289.3	289.1	286.1	DNR	282.9	289.2	289.1	289.0	290.1
SW CRE	− 46[a], − 47[b]	− 54.6	− 53.1	− 46.3	− 44.8	DNR	− 40.8	− 49.3	− 47.8	− 47.2	− 45.5
LW up (OLR) all-sky	− 240[a], − 239[b], − 238[c]	− 238.4	− 238.9	− 242.1	− 251.4	− 243.3	− 227.1	− 240.9	− 240.8	− 242.5	− 250.0
LW up (OLR) clear-sky	− 268[a], − 267[b]	− 267.3	− 266.2	− 264.0	− 265.9	DNR	− 260.4	− 264.0	− 265.0	− 268.2	− 266.3
LW CRE	28[a], 28[b]	28.9	27.3	21.9	14.5	DNR	33.2	23.1	24.2	25.7	16.3
Net CRE	− 18[a], − 19[b]	− 25.8	− 25.8	− 24.4	− 30.3	DNR	− 7.6	− 26.2	− 23.7	− 21.5	− 29.3
Imbalance	0.7 [a]	− 4.0	− 2.8	0.7	− 10.1	− 6.8	14.9	− 1.0	0.4	− 0.6	− 5.4
Atmosphere											
SW absorbed all-sky	80[b]. 74[c], 77[d]	71.5	71.5	79.0	77.5	75.7	77.4	77.6	77.4	72.7	78.4
SW absorbed clear-sky	73[b], 73[d]	70.0	69.9	76.5	71.3	DNR	74.1	74.4	74.5	70.2	74.4
SW CRE	7[b], 4[d]	1.5	1.6	2.5	6.2	DNR	3.3	3.2	2.9	2.5	4.0
LW net all-sky	− 183 [b], − 180[c], − 187[d]	− 176.6	− 177.7	− 184.2	− 189.9	− 186.6	− 170.4	− 182.2	− 180.9	− 178.7	− 189.3
LW net clear-sky	− 183[b], − 184[d]	− 183.3	− 182.8	− 181.4	− 180.3	DNR	− 182.4	− 178.9	− 179.3	− 182.8	− 181.2
LW CRE	0[b], − 3[d]	6.8	5.1	− 2.8	− 9.6	DNR	12.0	− 3.3	− 1.6	4.1	− 8.1
Net CRE	7[b], 1[d]	8.2	6.7	− 0.2	− 3.4	DNR	15.2	0.0	1.3	6.5	− 4.1

Table 1 (continued)

Energy balance component	Reference Estimates Wm^{-2}	MERRA-2 Wm^{-2}	M2AMIP Wm^{-2}	ERA5 Wm^{-2}	JRA-55 Wm^{-2}	NCEP-R2 Wm^{-2}	20CRv3 Wm^{-2}	ERA20C Wm^{-2}	ERA20CM Wm^{-2}	MERRA Wm^{-2}	**JRA-3Q** Wm^{-2}
Surface											
SW down all-sky	185 [b], 186 [c], 187[d]	186.0	188.2	188.1	189.4	187.5	¨193.0	187.8	189.3	192.7	189.6
SW up all-sky	− 25 [b], − 22[c], − 23[d]	23.2	23.6	24.3	25.6	26.7	28.2	25.4	25.5	23.6	23.4
SW absorbed all-sky	160 [b], 164 [c], 164[d]	162.8	164.6	163.8	163.8	160.8	164.7	162.4	163.8	169.1	166.2
SW down clear-sky*	247[b], 244[d]	250.1	250.8	244.2	248.3	DNR	244.6	248.6	247.9	249.5	246.1
SW up clear-sky*	33[b], 30[d]	− 31.2	− 31.4	− 31.6	− 33.5	DNR	− 35.8	− 33.7	− 33.3	− 30.6	− 30.4
SW absorbed clear-sky	214[b], 214[d]	218.9	219.4	212.6	214.8	DNR	208.8	214.9	214.6	218.8	215.7
SW CRE	− 54[b], − 50 [d]	− 56.1	− 54.7	− 48.8	− 50.9	DNR	− 44.1	− 52.5	− 50.7	− 49.7	− 49.5
LW down all-sky	342[b], 341[c], 344[d]	336.4	337.1	339.5	338.1	340.9	341.1	337.6	336.8	334.9	339.5
LW up all/clear-sky	− 398[b], − 399[c], − 398[d]	− 398.2	− 398.4	− 397.4	− 399.6	− 397.6	− 397.9	− 396.3	− 396.7	− 398.6	− 400.2
LW net all-sky	− 56[b], − 58[c], − 54[d]	− 61.8	− 61.2	− 57.9	− 61.5	− 56.7	− 56.7	− 58.7	− 59.9	− 63.7	− 60.7
LW down clear-sky	314[b], 314[d]	314.3	315.0	314.8	314.0	DNR	319.9	311.2	311.0	313.2	315.1
LW net clear-sky	− 84[b], − 84[d]	− 83.9	− 83.4	− 82.6	− 85.6	DNR	− 78.0	− 85.1	− 85.7	− 85.4	− 85.1
LW CRE	28[b], 30[d]	22.1	22.2	24.7	24.1	DNR	21.3	26.4	25.8	21.7	24.4
Net CRE	− 26[b], − 20[d]	− 34.0	− 32.5	− 24.1	− 26.8	DNR	− 22.8	− 26.2	− 25.0	− 28.0	− 25.1
Net radiation	104[b], 106[c], 110[d]	101.0	103.4	105.9	102.3	104.1	108.0	103.6	103.9	105.4	105.5
Latent heat flux	− 82[b], − 81[c]	86.2	85.0	85.0	93.2	94.1	85.6	82.9	83.0	75.9	89.3
Sensible heat flux	− 21[b], − 25[c]	19.3	19.4	16.9	20.2	7.3	15.5	19.1	19.0	18.0	20.6
Surface Imbalance	0.6 [b], 0.5[c]	− 4.5	− 1.0	4.0	− 11.2	2.7	6.9	1.6	1.9	11.4	− 4.4

For related statistics on all-reanalyses means, inter-reanalyses spreads and standard deviations as well as respective reference estimates see Table 2. Not all reanalyses provide all energy balance components listed above, missing components are marked with DNR (Did Not Report). Units Wm^{-2}. Reference estimates from Loeb et al. (2018) ([a]), Wild et al. (2015/2019) ([b]), L'Ecuyer et al. (2015) ([c]) and Kato et al. (2018) ([d])

*Approximation only

3 Results

3.1 Shortwave Components

Table 1 presents global annual means of various TOA, atmospheric and surface energy balance components as estimated by the 10 reanalyses for the period 2001–2010, as well as recent reference estimates. As can be inferred from the first data row of Table 1, the reanalyses MERRA-2, M2AMIP, ERA5, ERA20C and ERA20CM consider the solar constant as 1361 Wm^{-2}. (The solar constant refers to the measured incoming shortwave radiation at the TOA per m^{-2} perpendicular to the incoming beam, which is four times higher than the same quantity per square meter on the Earth's sphere given in Table 1.) The value of 1361 Wm^{-2} is in line with the current best estimate of the solar constant based on the Solar Radiation and Climate Experiment (SORCE, Kopp and Lean 2011). However, the earlier reanalyses considered in this study (MERRA, JRA-55 and NCEP-R2) used an older and slightly higher estimate for the solar constant of 1365 Wm^{-2} considered as best estimate at the time of their production. The recent JRA-3Q reanalysis also still uses the older estimate of 1365 Wm^{-2}.

Figure 1 illustrates the global annual mean net shortwave radiation at the TOA (i.e., the total absorption of solar radiation in the climate system, upper panel), within the atmosphere (middle panel) and at the Earth's surface (lower panel) as represented in 10 reanalyses (red bars). Figure 1 and all subsequent bar-chart figures further include the mean over all 10 (9 for clear-sky) reanalyses (pink bars), the CMIP6 multi-model mean as given in Wild (2020) (green bars), observational references (black bars, taken from CERES-EBAF (Loeb et al. 2018) for the TOA fluxes and from Wild et al. (2015, 2019) for the surface, atmospheric and clear-sky fluxes, as well as a mean over the most recent reanalyses (blue bars). The latter consists of the most recent reanalyses provided by each institution performing reanalyses, namely the four reanalyses MERRA-2, ERA5, NCEP-R2 and JRA-3Q. This gives an indication how the contemporary generation of reanalyses represents to global mean energy balance components in comparison with previous generations and reference estimates.

Table 2 provides a summary of the related statistics in terms of all-reanalyses means, standard deviations and spreads (as defined here by the difference between the largest and smallest values). For comparison, Table 2 also contains the same statistics for the set of more than 30 CMIP6 climate models, which have been taken from Wild (2020), as well as the means over the 4 most recent reanalyses mentioned above (MERRA-2, ERA5, NCEP-R2 and JRA-3Q). Generally, the means over the recent 4 reanalyses are very similar to the means over all 10 reanalyses considered here, and within 2 Wm^{-2} for most of the components (Table 2).

The spread amongst the 10 different reanalyses in their global mean TOA, atmospheric and surface shortwave absorption estimates is fairly similar, between 7.5 Wm^{-2} (atmospheric absorption) and 10.2 Wm^{-2} (TOA absorption). Interestingly, the standard deviations of the reanalysis estimates for these components are not smaller than the corresponding ones of the CMIP6 models, or even slightly larger in case of the TOA and atmospheric absorption (Table 2). This applies also for various other energy balance components listed in Table 2 in terms of their climatological global means. Specifically, in 20 out of the 36 variables in Table 2 the standard deviation amongst the reanalysis estimates is larger than the comparable CMIP6 estimates. This suggests that the representation of the global energy balance components is generally not more consistent

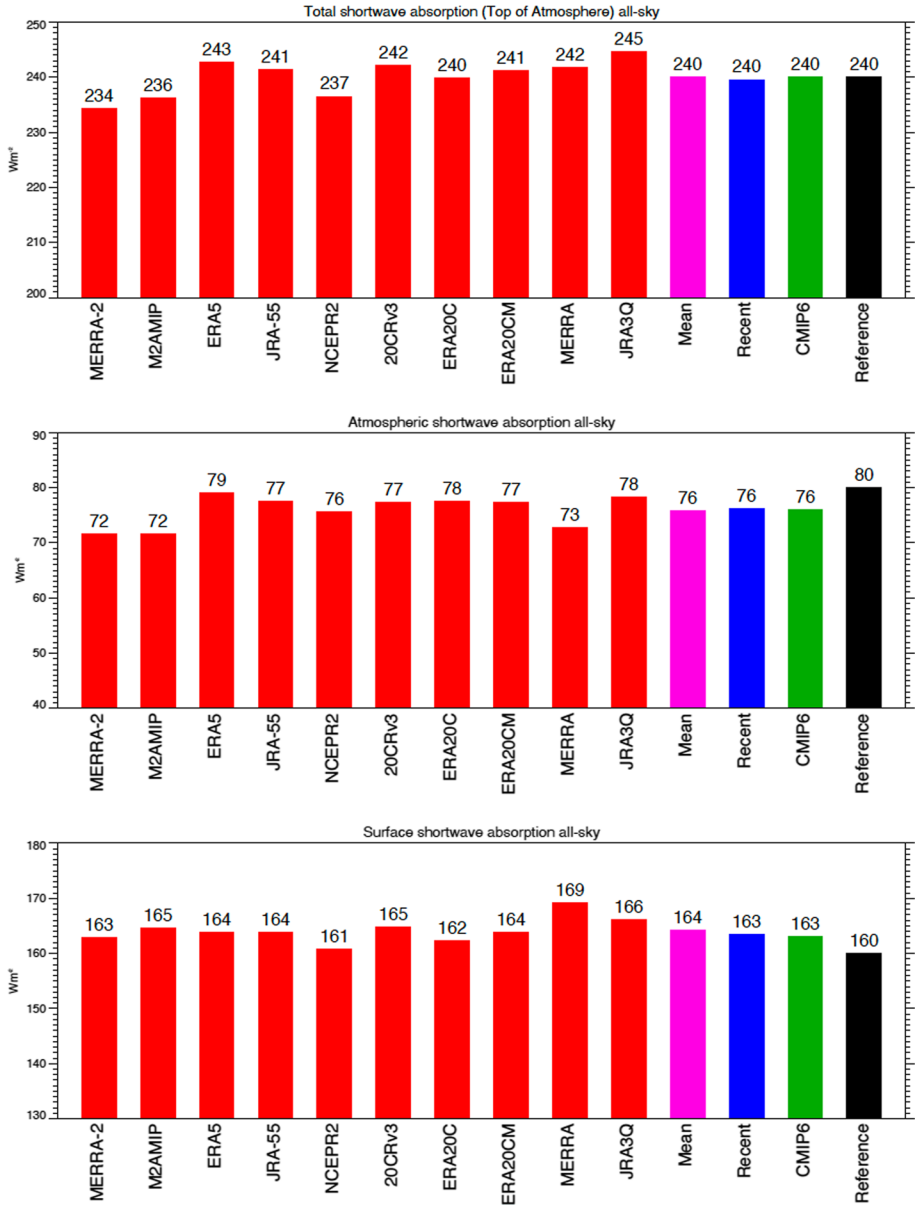

Fig. 1 Global annual mean shortwave all-sky radiation budgets representative for the period 2001–2010 as simulated by 10 different reanalyses (red bars), plus the mean over all 10 reanalyses (pink bar), the mean over the 4 most recent reanalyses (blue bar), the CMIP6 multi-model mean (green bar) and a reference estimate (black bar): shortwave radiation absorbed in the total climate system (TOA, upper panel), within the atmosphere (middle panel) and at the surface (lower panel). TOA reference estimates from the CERES-EBAF dataset (Loeb et al. 2018; Kato et al. 2018), atmospheric and surface reference estimates from Wild et al. (2015). Numbers above bars rounded to integers in Wm^{-2}

Table 2 Global annual means of various energy balance components at the TOA, within the atmosphere and at the surface under all-sky and clear-sky conditions from reanalyses, CMIP6 climate models and reference estimates, representative for the first decade of the twenty-first century (2001–2010)

Energy balance component	Reference Estimates Wm^{-2}	#Reanal (#CMIP6 Models)	Reanal mean Wm^{-2}	Reanal spread Wm^{-2}	Reanal stdev Wm^{-2}	CMIP6 mean Wm^{-2}	CMIP6 spread Wm^{-2}	CMIP6 stdev Wm^{-2}	Recent Reanal mean Wm^{-2}
TOA									
SW down	340[a], 340[b], 340[c]	10 (37)	340.8	1.0	0.5	340.2	5.3	0.9	340.9
SW up all-sky	−99[a], −100[b], −102[c]	10 (38)	−100.7	9.3	3.2	−100.6	13.1	2.7	−101.3
SW absorbed all-sky	241[a], 240[b], 238[c]	10 (37)	240.1	10.2	3.3	239.5	14.5	2.9	239.6
SW up clear-sky	−53[a], −53[b]	9 (37)	−52.5	6.3	2.3	−53.0	7.7	1.9	−51.3
SW absorbed clear-sky	287[a], 287[b]	9 (37)	288.2	7.2	2.3	287.3	7.1	1.8	289.4
SW CRE	−46[a], −47[b]	9 (37)	−47.7	13.8	4.2	−47.8	19.2	3.6	−48.8
LW up (OLR) all-sky	−240[a], −239[b], −238[c]	10 (40)	−241.5	24.2	6.6	−238.3	15.6	2.8	−243.4
LW up (OLR) clear-sky	−268[a], −267[b]	9 (38)	−265.2	7.8	2.3	−262.4	12.5	2.6	−265.8
LW CRE	28[a], 28[b]	9 (38)	23.9	18.7	5.9	24.1	10.4	2.3	22.4
Net CRE	−18[a], −19[b]	9 (37)	−23.8	22.6	6.6	−23.6	13.5	3.3	−26.5
Imbalance	0.7 [a]	(37)	−1.5	25.0	6.7	1.1	4.5	0.8	−3.9
Atmosphere									
SW absorbed all-sky	80[b]. 74[c], 77[d]	10 (37)	75.9	7.5	2.9	76.0	8.9	2.0	76.1
SW absorbed clear-sky	73[b], 73[d]	9 (36)	72.8	6.6	2.4	72.8	8.6	1.8	73.6
SW CRE	7[b], 4[d]	9 (36)	3.1	4.7	1.4	3.2	4.0	1.1	2.7
LW net all-sky	−183 [b], −180[c], −187[d]	10 (37)	−181.6	19.4	6.1	−182.1	17.2	4.2	−184.2
LW net clear-sky	−183[b], −184[d]	9 (33)	−181.4	4.4	1.6	−180.9	15.1	3.0	−182.0
LW CRE	0[b], −3[d]	9 (33)	0.3	21.6	7.1	−1.3	9.8	2.9	−1.4
Net CRE	7[b], 1[d]	9 (33)	3.4	19.3	6..3	1.9	10.0	2.6	1.3

Table 2 (continued)

Energy balance component	Reference Estimates Wm^{-2}	#Reanal (#CMIP6 Models)	Reanal mean Wm^{-2}	Reanal spread Wm^{-2}	Reanal stdev Wm^{-2}	CMIP6 mean Wm^{-2}	CMIP6 spread Wm^{-2}	CMIP6 stdev Wm^{-2}	Recent Reanal mean Wm^{-2}
Surface									
SW down all-sky	185 [b], 186 [c], 187[d]	10 (38)	189.2	6.9	2.2	187.4	20.8	4.5	187.8
SW up all-sky	−25 [b], −22[c], −23[d]	10 (37)	−25.0	5.1	1.6	−23.9	9.4	2.0	−24.4
SW absorbed all-sky	160 [b], 164 [c], 164[d]	10 (37)	164.2	8.3	2.3	163.4	12.1	3.0	163.4
SW down clear-sky*	247[b], 244[d]	9 (37)	247.8	6.6	2.4	244.8	15.4	2.8	246.8
SW up clear-sky*	33[b], 30[d]	9 (36)	32.4	5.4	1.8	30.2	12.7	2.3	31.0
SW absorbed clear-sky	214[b], 214[d]	9 (36)	215.3	6.8	2.7	214.6	11.0	2.2	215.8
SW CRE	−54[b], −50 [d]	9 (36)	−50.8	12.0	3.5	−51.2	20.4	4.0	−51.5
LW down all-sky	342[b], 341[c], 344[d]	10 (38)	338.2	6.3	2.0	343.8	20.3	5.2	339.1
LW up all-sky/ clear-sky	−398[b], −399[c], −398[d]	10 (37)	−398.1	3.9	1.2	−399.9	11.7	3.0	−398.3
LW net all-sky	−56[b], −58[c], −54[d]	10 (37)	−59.9	7.0	2.3	−56.2	14.0	3.6	−59.3
LW down clear-sky	314[b], 314[d]	9 (33)	314.3	8.9	2.6	318.0	22.5	5.1	314.7
LW net clear-sky	−84[b], −84[d]	9 (33)	−83.9	7.7	2.5	−81.7	16.1	3.5	−83.9
LW CRE	28[b], 30[d]	9 (33)	23.6	5.1	1.9	25.5	7.5	2.2	23.7
Net CRE	−26[b], −20[d]	9 (33)	−27.2	11.2	3.8	−25.4	15.3	3.6	−27.7
Net radiation	104[b], 106[c], 110[d]	10 (37)	104.3	6.9	2.0	107.2	13.1	3.1	104.1
Latent heat flux	−82[b], −81[c]	10 (38)	−86.0	18.2	5.3	−85.3	18.0	3.5	−88.7
Sensible heat flux	−21[b], −25[c]	10 (39)	−17.5	13.3	3.9	−20.1	13.2	2.7	16.0
Surface Imbalance	0.6 [b], 0.5[c]	10 (36)	0.7	22.6	6.4	1.5	1.2	0.3	−0.6

Given are means over up to 10 Reanalyes and 40 CMIP6 models together with their inter-model spreads as well as their standard deviations. "Reanal mean" is an average over all 10 (9) reanalyses considered in this study. "Recent Reanal mean" corresponds to an average over the most recent reanalyses (*MERRA-2, ERA5, NCEP-R2 and JRA-3Q).* Reanalyses results from the present study, CMIP6 results from Wild (2020). Reference estimates from Loeb et al. (2018) ([a]), Wild et al. (2015/2019) ([b]), L'Ecuyer et al. (2015) ([c]) and Kato et al. (2018) ([d])

*Approximation only

amongst the reanalyses than amongst the climate models. This might be somewhat surprising, given the fact that the atmospheric structure in the reanalyses is strongly constrained by the assimilated observations (except for the AMIP-type reanalysis runs of ERA20CM and MERRA-2 AMIP), in contrast to the "free-running" CMIP6 models, where not even the SSTs are observationally constrained but instead calculated by the coupled atmosphere–ocean ensemble modeling systems. Note, however, that climate models are typically tuned to match some of the observational reference quantities on a global mean level (Hourdin et al. 2017). This is particularly the case for their global mean TOA fluxes, which are usually tuned to match the satellite-based reference values from CERES-EBAF (Loeb et al. 2018). Reanalyses may also be tuned, however, while climate models can be integrated and reintegrated until the tuning converges on climate time scales, reanalysis systems in data assimilation mode can only be tuned for brief periods because of the computational demand. This may result in a less effective tuning, and may partly explain the similar or higher standard deviations of the reanalysis global mean energy balance components compared to the CMIP6 models. Also, changing observing systems can introduce spurious changes over time in reanalyses, which is not the case in free-running climate models.

In Table 2, one can further also see that the total spreads in the majority of the variables are still larger amongst the CMIP6 models than amongst the reanalyses, but this can be expected due to the many more CMIP6 models (33–40) than reanalyses (9–10) considered in this analysis.

The spread and standard deviation amongst the different reanalyses with respect to their global mean clear-sky net shortwave radiation at the TOA (i.e., the total solar absorption in the climate system under cloud-free conditions) are lower than their all-sky equivalents (Table 2, Fig. 2 upper panel). However, within the atmosphere and at the surface, the spreads and standard deviations of their clear-sky shortwave absorption are almost as large as the ones of their all-sky counterparts (Table 2, Fig. 2 middle and lower panels). This suggests that uncertainties in the partitioning of the shortwave absorption between atmosphere and surface cause similar discrepancies under clear-sky and all-sky conditions. The standard deviations in the shortwave clear-sky budgets of the reanalyses are also similar to the CMIP6 climate models (Table 2). The slightly larger standard deviation in the atmospheric clear-sky absorption in the reanalyses compared to the climate models might again be somewhat surprising, given the fact that the humidity, an essential absorber of shortwave radiation in the cloud-free atmosphere, is observationally constrained in the reanalyses, in contrast to the climate models. This may suggest that differences in the formulation of the radiation codes used in the reanalyses and climate models could be more relevant for the discrepancies in the radiative fluxes than differences in the physical atmospheric structure entering the radiation codes. Discrepancies could further also be enhanced by different treatments of absorbing aerosols or ozone in the reanalyses and climate models, as well as potential differences in the observational humidity inputs in the various reanalyses.

For the 9 reanalyses which provide both all-sky and clear-sky budgets, the global mean cloud radiative effect (CRE) can be diagnosed at the TOA, within the atmosphere and at the surface, as the difference between the global mean all-sky and clear-sky estimates (Tables 1, 2). The standard deviations of the global mean shortwave CREs amongst the reanalyses are again similar to the CMIP6 models (slightly larger at the TOA and in the atmosphere, while slightly smaller at the surface, Table 2).

With respect to the agreement with independent reference values, both the all-reanalyses means and the recent-reanalyses means are close to the reference estimates for most of their shortwave components, i.e., within 2 Wm^{-2} (Table 2).

At the TOA, the absorbed all-sky solar radiation averaged over all 10 reanalyses is in close agreement with the reference estimates from CERES-EBAF (Loeb et al. 2018), although favored by a small compensation between a slight overestimation of TOA clear-sky absorption and a slight overestimation of the reflectivity in cloudy conditions (i.e., a slightly too strong SW CRE (Table 2)). This applies even more so for the 4 recent-reanalyses mean (Table 2). As noted in Bosilovich et al. (2015), a low bias in the TOA all-sky shortwave absorption is evident in MERRA-2, on the order of 6 Wm^{-2}, whereas the recent JRA-3Q shows a high bias of similar magnitude in this quantity (Table 1, Fig. 1).

As already mentioned in Sect. 2, reference values for the shortwave absorption in the atmosphere and at the surface are less well established, since these quantities cannot be directly measured from satellites. Compared to our best estimate of 80 Wm^{-2} for the all-sky shortwave atmospheric absorption (Wild et al. 2015), the all- and recent-reanalyses means are, at 75.9 and 76.1 Wm^{-2} somewhat low, but still within the range of the observational references (Table 2). However, the entire MERRA reanalysis family (MERRA, MERRA-2 and MERRA-2 AMIP) tends to calculate a too transparent atmosphere for solar radiation under all-sky conditions compared to all reference estimates (Table 1). The spread in all-sky atmospheric absorption remains substantial also amongst the most recent reanalyses, ranging from 71.5 Wm^{-2} in MERRA-2 to 79.0 Wm^{-2} in ERA5 (Table 1).

Under cloud-free conditions, the atmospheric shortwave absorption in the all- and recent-reanalyses means nearly match the reference values of 73 Wm^{-2} (Table 2). Note also that the two reference estimates for this quantity in Table 2 (Kato et al. 2018; Wild et al. 2019) perfectly agree, despite their entirely different and independent derivations. With respect to the individual reanalyses, the MERRA family also systematically underestimates the global mean clear-sky shortwave atmospheric absorption, by 3 Wm^{-2}, whereas ERA5 overestimates this quantity by a similar amount.

When comparing the shortwave fluxes at the surface to the reference estimates, the all-reanalyses mean tends to overestimate the all-sky downward shortwave components, on the order of 3 Wm^{-2}, which is reinforced by the strong overestimation of the 20CRv3 and the older MERRA reanalyses, on the order of 7 Wm^{-2} (Tables 1, 2, Fig. 3 upper panel). This overestimation is partly caused by an overestimation of this quantity under cloud-free conditions (Table 1), and an underestimated all-sky absorption in the atmosphere (Fig. 1 middle panel) in some of the models. This applies again particularly to the MERRA family, which shows excessive global mean downward clear-sky shortwave fluxes (Table 1), in line with the overly low atmospheric clear-sky shortwave absorption mentioned above, as well as a somewhat high TOA clear-sky shortwave absorption (Fig. 2 upper and middle panels). In the case of MERRA-2 under all-sky conditions, the excessive clear-sky insolation is partly compensated by an excessive shortwave reflectance in cloudy areas (i.e., a too strong shortwave CRE, Table 1) as mentioned above. The excessive surface insolation due to an overly transparent atmosphere has been a long-standing issue over the history of climate model development (Wild et al. 1995; Wild 2008). It has been partly attributed to the lack of water vapor absorption in the atmosphere due to deficiencies in the related spectroscopic absorption coefficients and in the formulations of the near-infrared water vapor continuum used in the radiation codes (Morcrette 2002; Paynter and Ramaswamy 2012, 2014; Pincus et al. 2015; Radel et al. 2015). Deficiencies in shortwave atmospheric absorption have also been noted in the CMIP5 models in DeAngelis et al. (2015), which have been alleviated in the some of the CMIP6 models (Pendergrass 2020; Wild 2020).

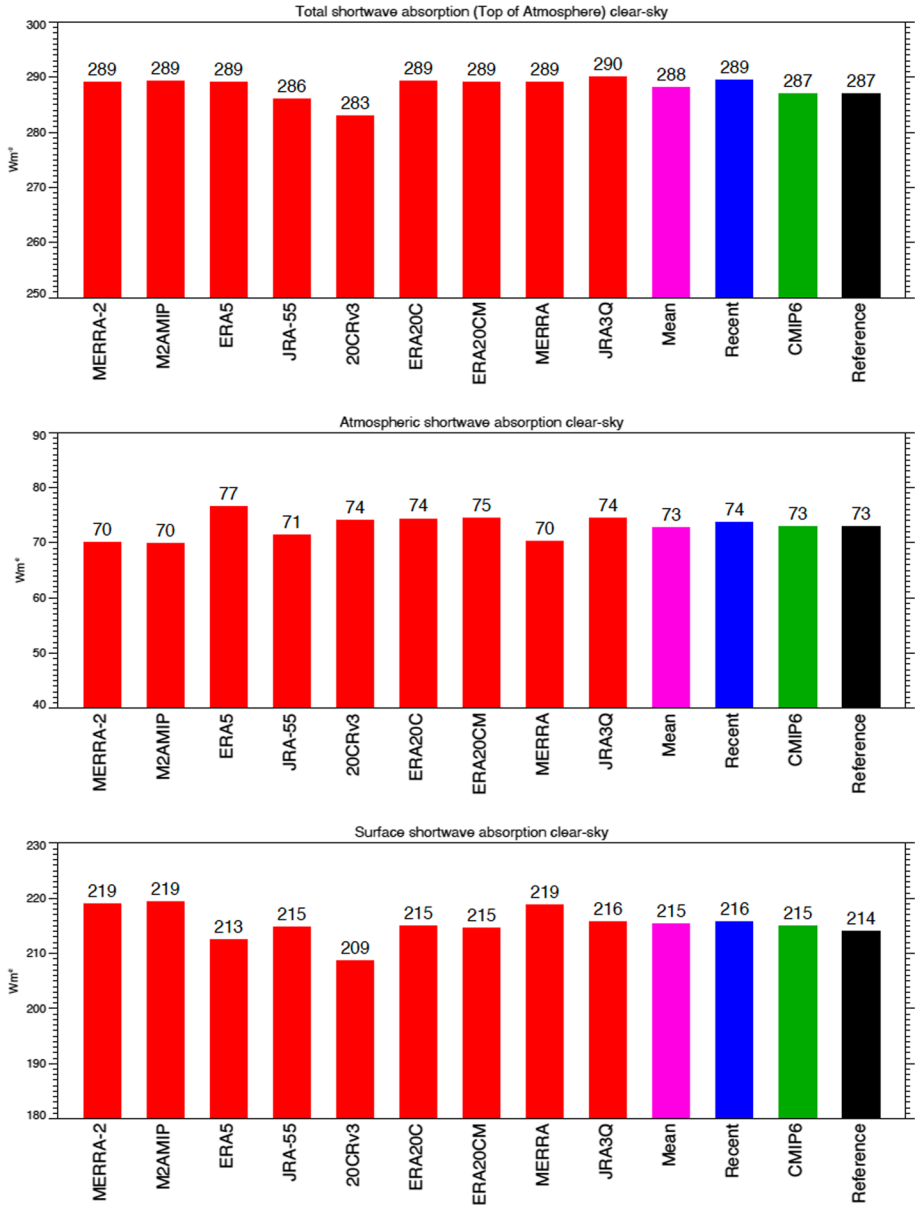

Fig. 2 as Fig. 1, but for clear-sky shortwave budgets of 9 different reanalyses. TOA reference estimates from the CERES-EBAF dataset (Loeb et al. 2018), atmospheric and surface reference estimates from Wild et al. (2019)

Generally, compared to the CMIP6 multi-model means, the shortwave components in the all- and recent-reanalyses means are not closer to the reference estimates neither under all-sky nor under clear-sky conditions.

3.2 Longwave Components

Figures 4 and 5 illustrate the global annual means of the net longwave radiation at the surface (lower panel), within the atmosphere (middle panel) and at the TOA (outgoing longwave radiation, OLR, upper panel), under all-sky and clear-sky conditions, respectively, as given by the different individual reanalyses, their all- and recent-reanalyses means, the CMIP6 multi-model means and the reference estimates. As in the shortwave, several of the longwave components including the longwave CREs determined by the reanalyses show similar or larger standard deviations and spreads than the ones simulated by the CMIP6 models (Table 2). This applies for example to the global mean all-sky OLR, with a spread amongst the reanalyses of as much as 24.2 Wm^{-2}, corresponding to 10% of the absolute magnitudes, and a standard deviation of 6.6 Wm^{-2}. This is partly due to the exceptionally low all-sky OLR in the 20CRv3 reanalysis (Fig. 4). Also in the TOA longwave CRE, the spread and standard deviation is substantial, at 18.7 and 5.9 Wm^{-2}, respectively, reinforced by the particularly low and high TOA longwave CRE in JRA-55 and 20CRv3, respectively. This causes the reanalysis spread to be considerably larger than amongst the many more CMIP6 models (Table 2). This similarly applies to the longwave CRE in the atmosphere, which shows, at 21.6 Wm^{-2}, a much larger spread amongst the 9 reanalyses than amongst the 33 CMIP6 models with a spread of 9.8 Wm^{-2}.

The longwave clear-sky components, on the other hand, show generally a higher consistency in the reanalyses compared to the CMIP6 models. This is likely due to the observationally constrained temperature and water vapor profiles in the former, which are particularly relevant for the determination of the longwave clear-sky fluxes.

With respect to the longwave reference estimates, at the TOA, both all- and recent-reanalyses means slightly overestimate and underestimate the global mean OLR under all-sky and clear-sky conditions, respectively, compared to the CERES-EBAF estimates. This leads to a too weak global mean TOA longwave CRE (Table 2) in the all- and recent-reanalyses means, on the order of 4 and 6 Wm^{-2}, respectively. As mentioned above, the spread amongst the individual reanalyses in this quantity is, however, substantial.

At the surface, a noteworthy feature is the somewhat low global mean downward longwave radiation in the all- and recent-reanalyses means compared to the reference estimates. Specifically, compared to our best estimate (Wild et al 2013, 2015), the all-reanalyses mean is low by 4 Wm^{-2}, while by 3 Wm^{-2} for the recent-reanalysis mean (Table 2, Fig. 3 lower panel). Also, all individual reanalyses shown in Fig. 3 (lower panel) calculate a global mean downward longwave radiation that is up to 5 Wm^{-2} lower than the lowest reference estimate, or at best equal to the lowest reference estimate (NCEP-R2 and 20CRv3 at 341 Wm^{-2}). In some of the reanalyses, the underestimation is also evident under clear-sky conditions (Table 2). The underestimation of the downward longwave radiation, similarly as the overestimation of the downward shortwave radiation discussed in the previous section, is a long-standing issue in numerical models of weather and climate (Wild et al. 1995, 2001). This underestimation has been partly related to uncertainties in the formulation of the longwave water vapor continuum (Iacono et al. 2000; Paynter and Ramaswamy 2011; Wild et al. 2001). Over generations of weather and climate models, the underestimation of the downward longwave radiation has compensated for the overestimation of the downward shortwave radiation, leading to a superficially correct surface net radiation in the global mean due to error compensation (Wild et al. 1995, 2013; Wild 2008). The situation has gradually improved over time (Wild 2020), but seems to remain an issue in some of the reanalyses.

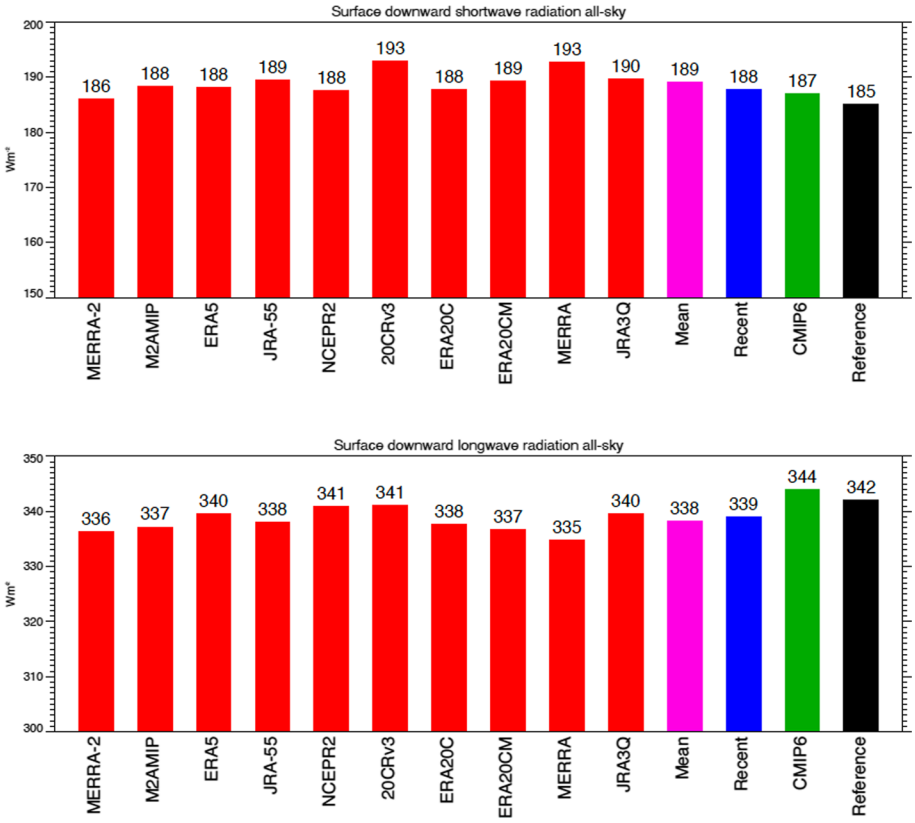

Fig. 3 Global annual mean all-sky downward shortwave (upper panel) and longwave (lower panel) radiation at Earth's surface representative for the period 2001–2010 as simulated by 10 different reanalyses (red bars), plus the mean over all 10 reanalyses (pink bar), the mean over the 4 most recent reanalyses (blue bar), the CMIP6 multi-model mean (green bar) and a reference estimate (black bar). Reference estimates from Wild et al. (2015). Numbers above bars rounded to integers. Units Wm^{-2}

3.3 Surface Net Radiation and Non-radiative Fluxes

Figure 6 displays the global mean surface net radiation (upper panel) as well as the non-radiative fluxes of surface latent and sensible heat (middle and lower panel, respectively) of the 10 reanalyses. In both all- and recent-reanalyses means, the global mean surface net radiation (also known as surface radiation balance) perfectly matches our best estimate of 104 Wm^{-2} (Wild et al. 2015) (Table 2). However, as noted above in Sects. 3.1 and 3.2, this overall good agreement is partly caused by an excessive downward solar radiation, which is compensated by a too weak downward longwave radiation. Thereby, also the individual reanalyses calculate magnitudes of global mean surface net radiation which are mostly within a few Wm^{-2} of our estimate. The largest compensation between overestimated downward shortwave and underestimated downward longwave radiation is found in the older MERRA reanalysis, with counteracting biases on the order of 8 Wm^{-2}. The same tendency, albeit with smaller biases is also found in JRA-55, JRA-3Q, M2AMIP, ERA20CM and ERA5, while NCEP2 shows hardly any biases in this respect. On the other

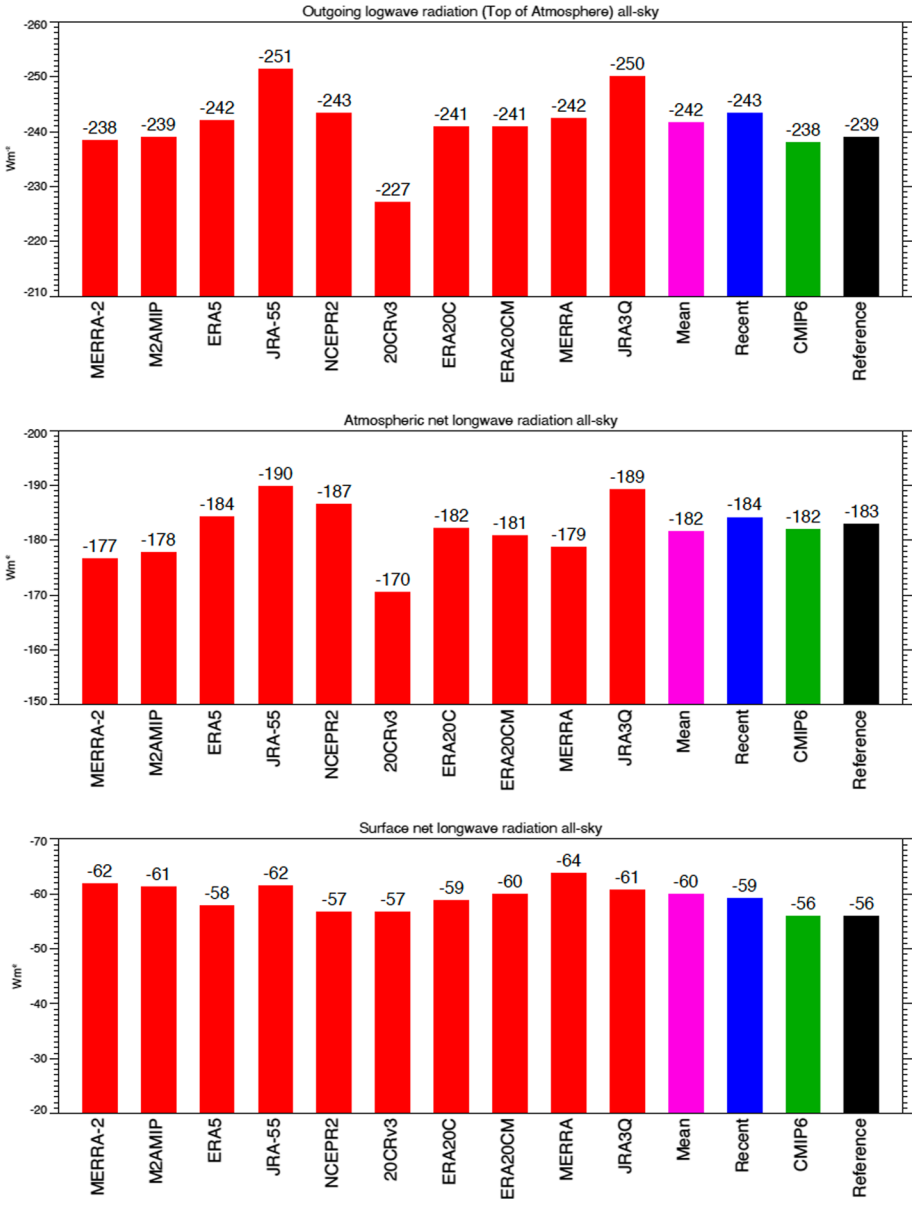

Fig. 4 Global annual mean longwave all-sky radiation budgets representative for the period 2001–2010 as simulated by 10 different reanalyses (red bars), plus the mean over all 10 reanalyses (pink bar), the mean over the 4 most recent reanalyses (blue bar), the CMIP6 multi-model mean (green bar) and a reference estimate (black bar): longwave radiation emitted to space (upper panel), net longwave radiation within the atmosphere (middle panel) and at the surface (lower panel). TOA reference estimates from the CERES-EBAF dataset (Loeb et al. 2018), atmospheric and surface reference estimates from Wild et al. (2015). Numbers above bars rounded to integers. Units Wm^{-2}

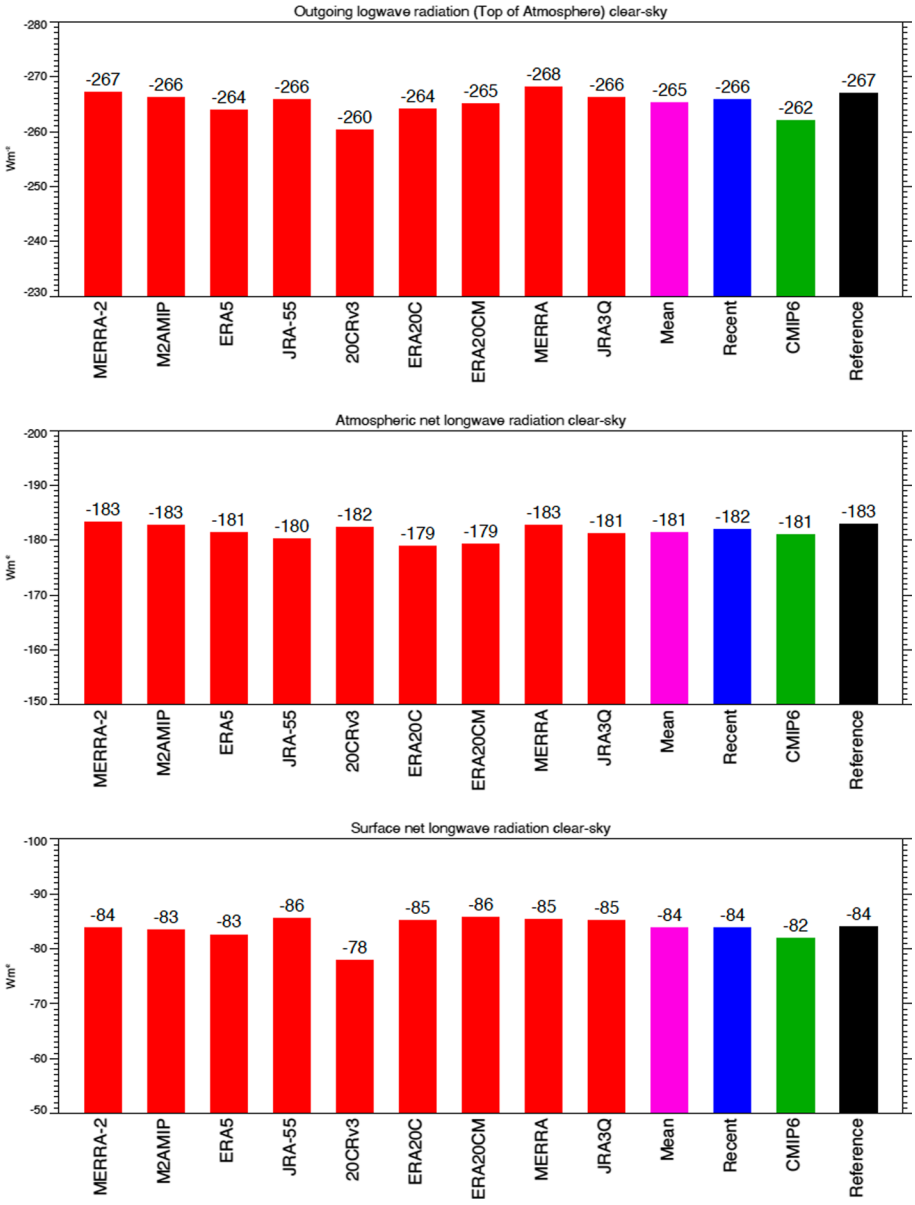

Fig. 5 As Fig. 4, but for clear-sky longwave budgets of 9 different reanalyses. TOA reference estimates from the CERES-EBAF dataset (Loeb et al. 2018), atmospheric and surface reference estimates from Wild et al. (2019)

hand, the somewhat low surface net radiation in MERRA-2 (101 Wm^{-2}) is primarily a consequence of a too low downward longwave radiation (336 Wm^{-2}). At the other end of the spectrum, the somewhat high surface net radiation of 108 Wm^{-2} in 20CRv3 is primarily induced by a too high downward solar radiation (193 Wm^{-2}), while the downward longwave radiation is, at 341 Wm^{-2}, in line with the reference estimates.

Despite the reasonably similar global mean surface net radiation and thus radiative energy available for evaporation at the surface in the 10 reanalyses, the global mean latent heat fluxes largely vary across the different reanalyses, in a range of as much as 18 Wm^{-2} (Fig. 6 middle panel). This spread is not smaller than the spread in the CMIP6 models, despite the much larger number of CMIP6 models than reanalyses considered here (Table 2). As a consequence, also the representation of the global water cycle largely differs in the various reanalyses. Since the latent heat flux varies across the reanalyses by 21%, this implies that the global mean precipitation in the different reanalyses also varies by a similar amount (i.e., by more than 20%). A similarly large spread in global mean precipitation in earlier generation reanalyses can be inferred from Table 1 of Bosilovich et al. (2008). Still, it is noteworthy that several of the recent reanalyses show global mean latent heat flux values near 85 Wm^{-2}, in reasonable agreement with the reference estimates (Fig. 6 middle panel, Table 1).

The much larger spread and standard deviation in the latent heat flux than in the surface net radiation also indicates that the Bowen ratio (ratio between sensible and latent heat flux) varies considerably across the different reanalyses. Accordingly, also the global mean sensible heat flux in the different reanalyses shows a substantial spread, of 13.3 Wm^{-2}, corresponding to 75% of its absolute value (Table 2, Fig. 6 lower panel). This is largely caused by the very low sensible heat flux in NCEP2, whereas the other reanalyses tend to cluster around 19 Wm^{-2} in their global mean sensible heat fluxes. Due to the lack of widespread long-term direct observations of sensible heat fluxes and the considerable uncertainties in estimates from bulk parameterizations (Yu 2019), this quantity is poorly constrained and the available global mean reference estimates differ considerably (Trenberth et al. 2009; Berrisford et al. 2011; Wild et al. 2015). A detailed assessment of the turbulent surface fluxes in MERRA can be found in Roberts et al. (2012).

3.4 TOA and Surface Imbalance

To keep the Earth's climate system in equilibrium, the shortwave radiation absorbed by the climate system should match the outgoing longwave radiation at the TOA, i.e., the radiation balance at the TOA should be zero. However, due to anthropogenic climate change, a positive imbalance (nonzero TOA radiation balance) is expected to occur, which causes an accumulation of energy in the climate system (e.g., von Schuckmann et al. 2016; Hakuba et al. 2019; Hakuba et al. 2021; von Schuckmann et al. 2023). This imbalance (also known as Earth Energy Imbalance EEI) is estimated to be + 0.8 Wm^{-2} over the period 2006–2018, primarily inferred from measurements of the energy accumulation in the global oceans (Forster et al. 2021). However, in contrast to coupled atmosphere–ocean GCMs, in reanalyses the energy accumulation is not only governed by the TOA imbalance, but also influenced by the prescribed SSTs and the assimilated observational data, which can induce additional energy sources. Still, the examination of the imbalance in reanalyses is relevant, considering that they aim at reproducing the physical structure of the atmosphere as realistic as possible, and as such may also be thought to have a potential to realistically capture the imbalance. However, in both all- and recent-reanalyses means the imbalance at the TOA is, at − 1.5 and − 3.9 Wm^{-2}, respectively, of opposite sign compared to any published TOA imbalance reference estimate (Table 2). This suggests that current reanalyses may not be able to serve as alternative pathways to better constrain the magnitude of the TOA imbalance, despite their incorporation of comprehensive observational data. With respect to the individual reanalyses, only ERA5 and ERA20CM simulate TOA imbalances, at 0.7

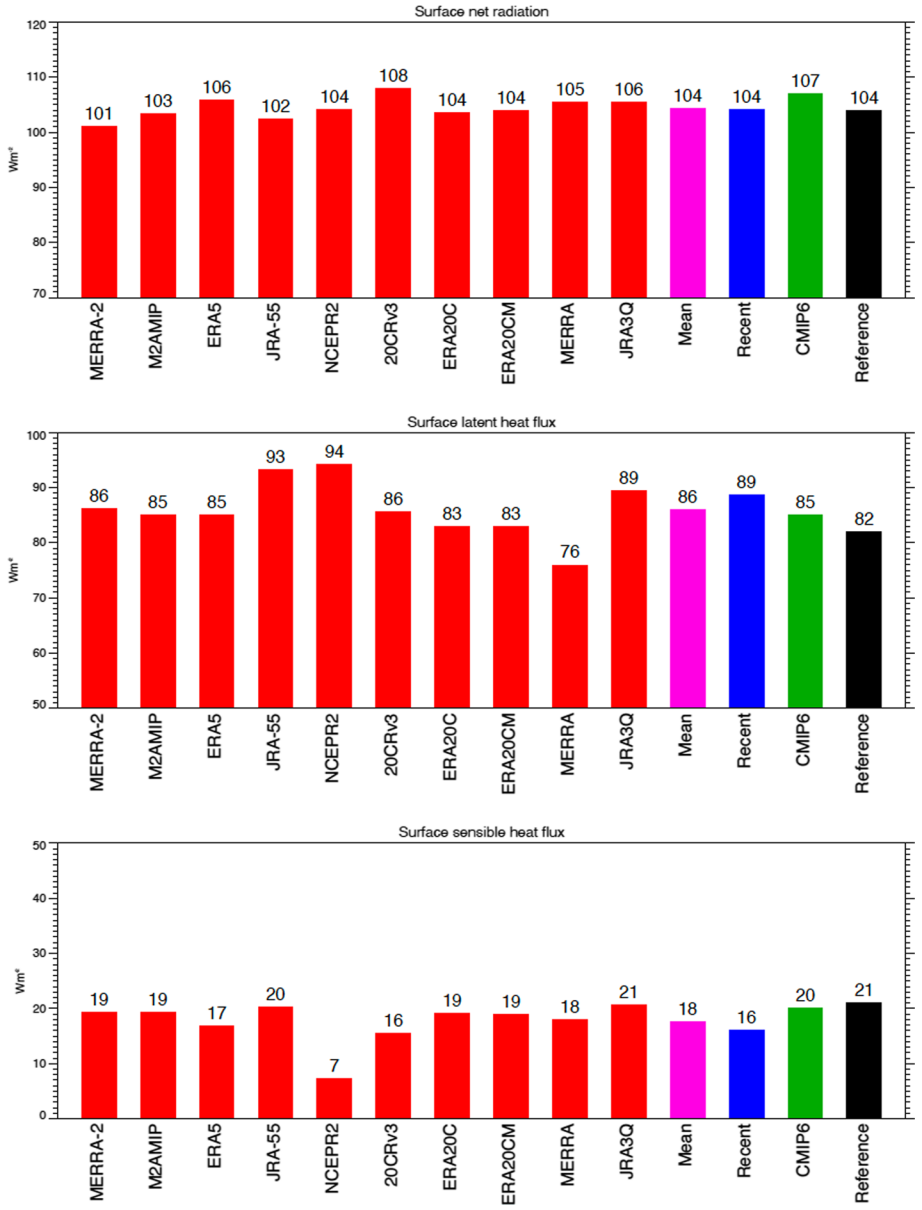

Fig. 6 Global annual mean surface net radiation (upper panel), latent heat fluxes (middle panel) and sensible heat fluxes (lower panel) representative for present-day climate as calculated by 10 different reanalyses (red bars), plus the mean over all 10 reanalyses (pink bar), the mean over the 4 most recent reanalyses (blue bar), the CMIP6 multi-model mean (green bar) and a reference estimate (black bar) from Wild et al. (2015). Numbers above bars rounded to integers. Units Wm^{-2}

and 0.4 Wm^{-2}, respectively, which are compatible with reference estimates and associated uncertainty ranges (Fig. 7 upper panel, Table 1, see also discussion in Hersbach et al. (2020), Sect. 6.1).

Also, the temporal change of the TOA imbalance is not adequately represented in the reanalyses (Fig. 8). While the annual imbalance in the CERES satellite data shows a dramatic increase over the first two decades of the twenty-first century as pointed out by Loeb et al. (2021) (thick black line in Fig. 8), only the JRA-3Q shows a slight increase, yet of an order of magnitude smaller than the CERES reference trend. All other reanalyses which cover the first two decades of the twenty-first century show a negative trend (linear trend magnitudes given in Fig. 8) and thus fail to capture the increasing energy imbalance in the climate system. The lack of a significant positive global mean trend in the ERA5 reanalysis and a related AMIP version is also documented in Table 1 of Loeb et al. (2022). Further with respect to ERA5, the lack of increase has been related to the TOA shortwave reflectance, which does not show the substantial decrease seen in CERES-EBAF, possibly related to the deficient representation of the decline in aerosol (Hodnebrog et al. 2024; Liu et al. 2020). Finally, climate models also underestimate the CERES trend by half (Schmidt et al. 2023), and seemingly the data assimilation in reanalysis systems does not appear to overcome this general modeling deficiency.

The lower panel of Fig. 7 shows the annual mean energy imbalance at the Earth's surface of the different reanalyses. This surface imbalance is deduced here from the difference between the surface net radiation and the sum of the surface sensible and latent heat fluxes. This roughly corresponds to the net energy flux into the oceans, because the amount of energy going into land surface and the melting of snow and ice are much smaller in comparison. The surface imbalance is thus quantitatively closely related to the TOA energy imbalance discussed above, since the energy storage in the atmosphere is small. In contrast to the CMIP6 models, where all 36 models show a positive surface imbalance as expected with increasing greenhouse-gas forcing (Wild 2020), 4 out of the 10 reanalyses show a negative surface imbalance (Fig. 7 lower panel). Both spread and standard deviation across the 10 reanalyses, at 22.6 and 6.4 Wm^{-2}, respectively, are massively larger (more than an order of magnitude) than across the 36 CMIP6 models, at 1.2 and 0.3 Wm^{-2}, respectively. There is also limited correlation in the reanalyses between their TOA and surface imbalances, which points to the effect of observational assimilation, where the correction of state variables (temperature and water vapor) by observations each day causes subsequent variations in the energy balance (see also Hersbach et al. 2020).

4 Discussion and Conclusions

In this study, the global mean energy balance components of 10 atmospheric reanalyses, representative for the period 2001–2010, have been intercompared and related to available reference estimates. Figure 9 provides an illustrative summary of the magnitudes of the global mean energy balance components according to the all-reanalyses mean and the corresponding values from the CMIP6 multi-model mean as well as the reference estimates from Kato et al. (2018) and Wild et al. (2015, 2019). Depicted are the values for both for all-sky and clear-sky conditions (Fig. 9 upper and lower panel, respectively).

The majority of the reanalyses considered in this study incorporate a comprehensive observational data assimilation (including prescribed observational SSTs), whereas two reanalysis models are only constrained by observed SSTs. To this end, it is interesting to compare the energy balance components of MERRA-2 and MERRA-2 AMIP, where the

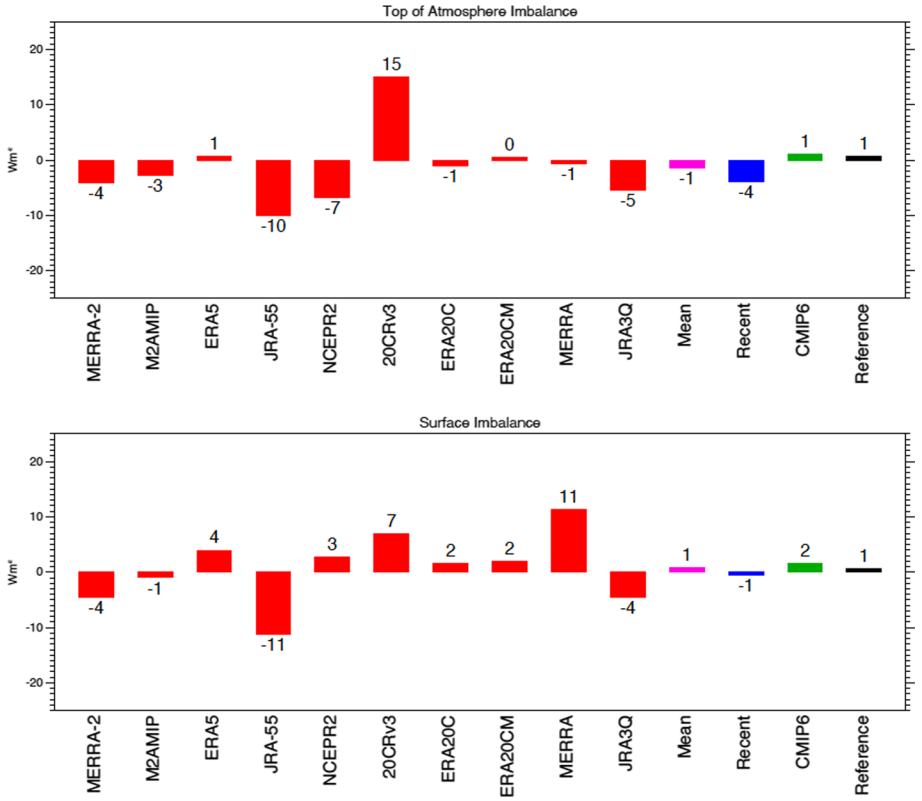

Fig. 7 Global annual mean energy imbalance at the TOA (upper panel) and at the Earth's surface (lower panel) for the period 2001–2010 estimated by 10 different reanalyses (red bars), plus the mean over all 10 reanalyses (pink bar), the mean over the 4 most recent reanalyses (blue bar), the CMIP6 multi-model mean (green bar) and a reference estimate (black bar). TOA energy imbalance determined as difference between absorbed shortwave radiation in the climate system (Fig. 1 upper panel) and the longwave emission to space (Fig. 4 upper panel). Surface imbalance determined as difference between surface net radiation (Fig. 6 upper panel) and the sum of surface sensible and latent heat fluxes (Fig. 6 middle/lower panels). Reference estimates from Forster et al. (2021). Numbers above bars rounded to integers. Units Wm^{-2}

same model is once run in full assimilation mode (MERRA-2), and once only constrained by the evolving SSTs (MERRA-2 AMIP). As can be inferred from Table 1 (columns 2 and 3), for most quantities the differences between the two realizations over the identical period 2001–2010 are within 2 Wm^{-2} for their global means. Exceptions are the surface downward shortwave radiation, the surface net radiation and the surface imbalance, where the differences amount to 2.2, 2.4 and 3.5 Wm^{-2}, respectively. The differences in the surface downward shortwave and net radiation come primarily from a stronger shortwave cloud radiative effect in the assimilated realization, which reduces the surface insolation, in better agreement with the reference estimates. In this case, the assimilation of observational data seems to have been beneficial, whereas for most other energy balance quantities the impact of the assimilation has been negligible in the global mean. Differences in the clear-sky fluxes between the two realizations tend to be particularly small and are typically within a few tenths of one Wm^{-2}. The surface imbalance in the assimilated realization is even less realistic and more negative than in the realization constrained by SSTs only. A similar

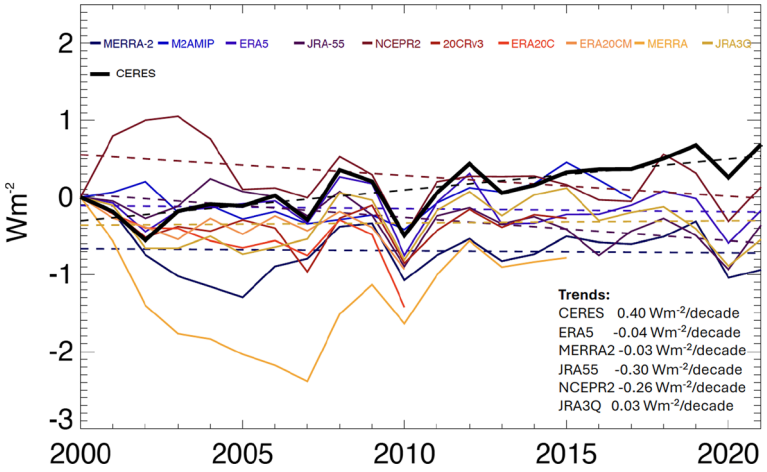

Fig. 8 Temporal evolution of the global annual mean TOA radiation balance (Earth energy imbalance EEI) as derived from the CERES-EBAF satellite dataset (Loeb et al. 2018) (black line) and as calculated in 10 different reanalyses (colored lines) over the first two decades of the twenty-first century. Shown are annual anomalies with respect to the beginning of the twenty-first century. Unit on vertical axis is Wm^{-2}. Linear trend magnitudes are given for CERES and for those 5 reanalyses which cover the entire first two decades of the twenty-first century

comparison can be made between ERA20C and ERA20CM, where ERA20C assimilates surface observations in addition to SSTs, whereas ERA20CM is only constrained by SSTs. Except for the net CRE at the TOA, all quantities in Table 1 differ by less than 2 Wm^{-2} between ERA20C and ERA20CM.

These comparisons suggest that the assimilation of observations does not substantially modify the overall representation of the global energy balance in reanalyses. This fits to the general picture portrayed here, in that the representation of the global energy balance components in reanalyses, despite the assimilation of observational data, is not obviously improved compared to the less constrained CMIP6 climate models. This generally also applies for the most recent reanalyses considered in this study (MERRA-2, ERA5, NCEP-R2 and JRA-3Q). We also showed that the consistency between the magnitudes of the global mean energy balance components in the different reanalyses is not necessarily higher than in the CMIP6 models, despite the additional observational constraints. This indicates that the magnitude of the global energy balance components in reanalysis systems, as in climate models, may depend more on the formulation of the specific parameterization schemes (i.e., the radiation codes for the radiative components) than on degree of observational constraints applied to the inputs to these schemes. In this respect, the reanalysis energy balance components are similarly prone to some of the well-known deficiencies in climate models. Specifically, we noted the tendency of an overestimated surface downward shortwave radiation globally, compensated by an underestimated surface downward longwave radiation, a long-standing issue in climate models, to be similarly present in the reanalyses. This compensational effect between the overestimated downward shortwave and underestimated downward longwave radiation, however, only works on a global annual mean basis, and does not apply on regional, seasonal and diurnal scales, thereby likely inducing biases on any of these scales. This should apply similarly to both reanalyses

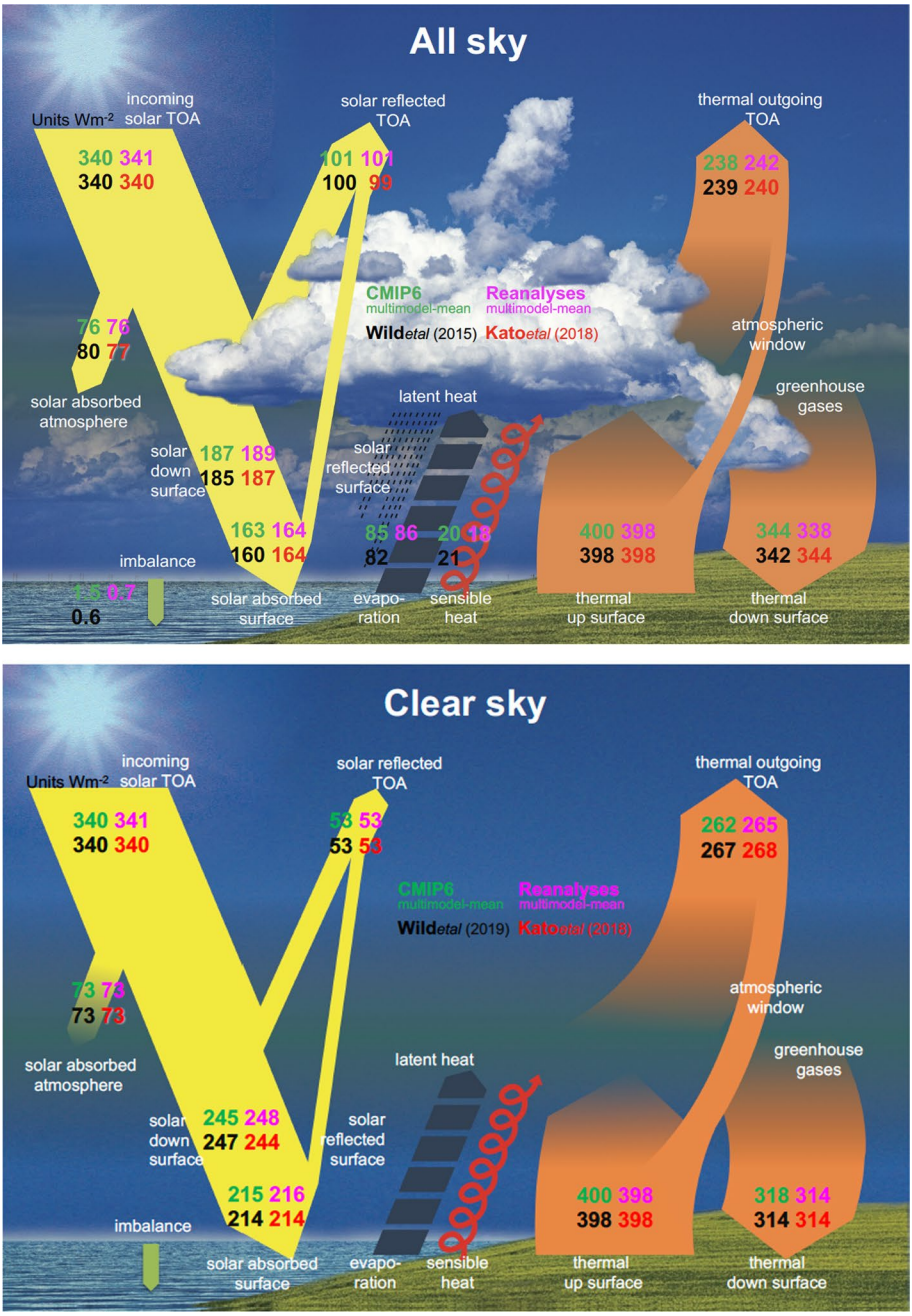

Fig. 9 Magnitudes of the different global annual mean energy balance components at the beginning of the twenty-first century under "all-sky" (upper panel) and "clear-sky" (lower panel) conditions, as simulated in the all-reanalyses mean (upper right (pink) values) and in the CMIP6 multi-model mean (upper left (green) values), and estimated by Wild et al. (2015, 2019) (lower left (black) values) and Kato et al. (2018) (lower right (red) values). Units Wm^{-2}

and climate models. Noteworthy is also the substantial spread in the intensity of the global water cycle between some of the reanalyses, as indicated by their largely diverging global mean surface latent heat fluxes. Also, current reanalyses cannot provide additional constraints on the magnitude of the Earth energy imbalance nor on its temporal evolution, since their absolute magnitudes as well as the sign of their trends are mostly unrealistic.

This does not put in question in any way the tremendous value of reanalyses for a wide range of applications. Reanalysis fields, such as geopotential height, upper air temperature, velocity or humidity fields have been most successfully used over many years as reliable references in countless studies. With respect to the different global energy balance components, however, it is not recommended to rely on currently available reanalyses as references.

Acknowledgements This paper is an outcome of the Workshop "Challenges in Understanding the Global Water Energy Cycle and its Changes in Response to Greenhouse Gas Emissions" held at the International Space Science Institute (ISSI) in Bern, Switzerland (26–30 September 2022). We are most grateful to the different institutions which engage in the enormous task of performing reanalyses. Research on the global energy balance at ETH Zurich is supported by the Swiss National Science Foundation, Grant No. 200020_188601, and at GSFC by the NASA Energy and Water cycle Studies (NEWS) program. We would like to thank also Richard Allan and 3 additional anonymous reviewers for their very constructive and helpful comments.

Funding Open access funding provided by Swiss Federal Institute of Technology Zurich.

Declarations

Conflict of interest The authors have no relevant financial or non-financial interests to disclose.

References

Allan RP, Liu CL, Loeb NG, Palmer MD, Roberts M, Smith D, Vidale PL (2014) Changes in global net radiative imbalance 1985–2012. Geophys Res Lett 41(15):5588–5597. https://doi.org/10.1002/2014gl060962

Allan RP, Ringer MA, Pamment JA, Slingo A (2004) Simulation of the earth's radiation budget by the european centre for medium-range weather forecasts 40-year reanalysis (era40). J Gerontol Ser A Biol Med Sci 109(D18):D18107. https://doi.org/10.1029/2004jd004816

Berrisford P, Kallberg P, Kobayashi S, Dee D, Uppala S, Simmons AJ, Poli P, Sato H (2011) Atmospheric conservation properties in era-interim. Q J R Meteorol Soc 137(659):1381–1399. https://doi.org/10.1002/Qj.864

Bosilovich MG, Akella S, Coy L, Cullather R, Draper C, Gelaro R, Kovach R, Liu Q, Molod A, Norris P, Wargan K, Chao W, Reichle R, Takacs L, Vikhliaev Y, Bloom S, Collow A, Firth S, Labow G, Partyka G, Pawson S, Reale O, Schubert SD, Suarez M (2015) Merra-2: Initial evaluation of the climate. NASA/TM–2015–104606 43:145

Bosilovich MG, Chaudhuri AH, Rixen M (2013) Earth system reanalysis: progress, challenges, and opportunities. Bull Am Meteorol Soc 94(8):Es110–Es113. https://doi.org/10.1175/Bams-D-12-00191.1

Bosilovich MG, Chen JY, Robertson FR, Adler RF (2008) Evaluation of global precipitation in reanalyses. J Appl Meteorol Clim 47(9):2279–2299. https://doi.org/10.1175/2008jamc1921.1

Bosilovich MG, Robertson FR, Chen JY (2011) Global energy and water budgets in merra. J Clim 24(22):5721–5739. https://doi.org/10.1175/2011jcli4175.1

Collow, Marquardt AB, Mahanama SP, Bosilovich MG, Koster RD, Schubert SD (2017) An evaluation of teleconnections over the united states in an ensemble of amip simulations with the merra-2 configuration of the geos atmospheric model. NASA/TM-2017–104606 47:68

DeAngelis AM, Qu X, Zelinka MD, Hall A (2015b) An observational radiative constraint on hydrologic cycle intensification. Nature 528(7581):249. https://doi.org/10.1038/nature15770

Forster P, Storelvmo T, Armour K, Collins W, Dufresne J-L, Frame D, Lunt DJ, Mauritsen T, Palmer MD, Watanabe M, Wild M, Zhang H (2021) The earth's energy budget, climate feedbacks, and climate sensitivity. In: V M-D, Zhai P, Pirani A et al. (eds) Climate change 2021: The physical science basis. Contribution of working group 1 to the sixth assessment report of the intergovernmental panel on climate change. Cambridge University Press, Cambridge, , United Kingdom and New York, NY, USA, pp 923–1054. https://doi.org/10.1017/9781009157896.009

Gelaro R, McCarty W, Suárez MJ, Todling R, Molod A, Takacs L, Randles CA, Darmenov A, Bosilovich MG, Reichle R, Wargan K, Coy L, Cullather R, Draper C, Akella S, Buchard V, Conaty A, da Silva AM, Gu W, Kim GK, Koster R, Lucchesi R, Merkova D, Nielsen JE, Partyka G, Pawson S, Putman W, Rienecker M, Schubert SD, Sienkiewicz M, Zhao B (2017) The modern-era retrospective analysis for research and applications, version 2 (merra-2). J Clim 30(14):5419–5454. https://doi.org/10.1175/Jcli-D-16-0758.1

Hakuba MZ, Frederikse T, Landerer FW (2021b) Earth's energy imbalance from the ocean perspective (2005–2019). Geophys Res Lett 48(16):e2021GL93624. https://doi.org/10.1029/2021GL093624

Hakuba MZ, Stephens GL, Christophe B, Nash AE, Foulon B, Bettadpur SV, Tapley BD, Webb FH (2019) Earth's energy imbalance measured from space. Ieee T Geosci Remote 57(1):32–45. https://doi.org/10.1109/Tgrs.2018.2851976

Hatzianastassiou N, Matsoukas C, Hatzidimitriou D, Pavlakis C, Drakakis M, Vardavas I (2004) Ten year radiation budget of the earth: 1984–93. Int J Climatol 24(14):1785–1802. https://doi.org/10.1002/joc.1110

Hersbach H, Bell B, Berrisford P, Hirahara S, Horányi A, Muñoz-Sabater J, Nicolas J, Peubey C, Radu R, Schepers D, Simmons A, Soci C, Abdalla S, Abellan X, Balsamo G, Bechtold P, Biavati G, Bidlot J, Bonavita M, De Chiara G, Dahlgren P, Dee D, Diamantakis M, Dragani R, Flemming J, Forbes R, Fuentes M, Geer A, Haimberger L, Healy S, Hogan RJ, Hólm E, Janisková M, Keeley S, Laloyaux P, Lopez P, Lupu C, Radnoti G, de Rosnay P, Rozum I, Vamborg F, Villaume S, Thépaut JN (2020) The era5 global reanalysis. Q J R Meteorol Soc 146(730):1999–2049. https://doi.org/10.1002/qj.3803

Hersbach H, Peubey C, Simmons A, Berrisford P, Poli P, Dee D (2015) Era-20cm: a twentieth-century atmospheric model ensemble. Q J R Meteorol Soc 141(691):2350–2375. https://doi.org/10.1002/qj.2528

Hodnebrog O, Myhre G, Jouan C, Andrews T, Forster PM, Jia HL, Loeb NG, Olivie DJL, Paynter D, Quaas J, Raghuraman SP, Schulz M (2024) Recent reductions in aerosol emissions have increased earth's energy imbalance. Commun Earth Environ 5(1):166. https://doi.org/10.1038/s43247-024-01324-8

Hourdin F, Mauritsen T, Gettelman A, Golaz JC, Balaji V, Duan QY, Folini D, Ji DY, Klocke D, Qian Y, Rauser F, Rio C, Tomassini L, Watanabe M, Williamson D (2017) The art and science of climate model tuning. Bull Am Meteor Soc 98(3):589–602. https://doi.org/10.1175/Bams-D-15-00135.1

Iacono MJ, Mlawer EJ, Clough SA, Morcrette JJ (2000) Impact of an improved longwave radiation model, rrtm, on the energy budget and thermodynamic properties of the ncar community climate model, ccm3. J Gerontol Ser A Biol Med Sci 105(D11):14873–14890

Kanamitsu M, Ebisuzaki W, Woollen J, Yang SK, Hnilo JJ, Fiorino M, Potter GL (2002) Ncep-doe amip-ii reanalysis (r-2). Bull Am Meteor Soc 83(11):1631–1643. https://doi.org/10.1175/Bams-83-11-1631(2002)083%3c1631:Nar%3e2.3.Co;2

Kato S, Rose FG, Rutan DA, Thorsen TJ, Loeb NG, Doelling DR, Huang X, Smith WL, Su WY (2018a) Surface irradiances of edition 40 clouds and the earth's radiant energy system (ceres) energy balanced and filled (ebaf) data product. J Clim 31(11):4501–4527

Kiehl JT, Trenberth KE (1997) Earth's annual global mean energy budget. Bull Am Meteor Soc 78(2):197–208

Kobayashi S, Ota Y, Harada Y, Ebita A, Moriya M, Onoda H, Onogi K, Kamahori H, Kobayashi C, Endo H, Miyaoka K, Takahashi K (2015) The jra-55 reanalysis: general specifications and basic characteristics. J Meteorol Soc Jpn 93(1):5–48. https://doi.org/10.2151/jmsj.2015-001

Kopp G, Lean JL (2011) A new, lower value of total solar irradiance: evidence and climate significance. Geophys Res Lett 38:L01706. https://doi.org/10.1029/2010gl045777

Kosaka Y, Kobayashi S, Harada Y, Kobayashi C, Naoe H, Yoshimoto K, Harada M, Goto N, Chiba J, Miyaoka K, Sekiguchi R, Deushi M, Kamahori H, Nakaegawa T, Tanaka TY, Tokuhiro T, Sato Y, Matsushita Y, Onogi K (2024) The jra-3q reanalysis. J Meteorol Soc Jpn 102(1):49–109. https://doi.org/10.2151/jmsj.2024-004

L'Ecuyer TS, Beaudoing HK, Rodell M, Olson W, Lin B, Kato S, Clayson CA, Wood E, Sheffield J, Adler R, Huffman G, Bosilovich M, Gu G, Robertson F, Houser PR, Chambers D, Famiglietti JS, Fetzer E, Liu WT, Gao X, Schlosser CA, Clark E, Lettenmaier DP, Hilburn K (2015) The observed state of the energy budget in the early twenty-first century. J Clim 28(21):8319–8346. https://doi.org/10.1175/Jcli-D-14-00556.1

Liu CL, Allan RP, Mayer M, Hyder P, Desbruyères D, Cheng LJ, Xu JJ, Xu F, Zhang Y (2020) Variability in the global energy budget and transports 1985–2017. Clim Dyn 55(11–12):3381–3396. https://doi.org/10.1007/s00382-020-05451-8

Liu CL, Allan RP, Mayer M, Hyder P, Loeb NG, Roberts CD, Valdivieso M, Edwards JM, Vidale PL (2017) Evaluation of satellite and reanalysis-based global net surface energy flux and uncertainty estimates. J Gerontol Ser A Biol Med Sci 122(12):6250–6272. https://doi.org/10.1002/2017jd026616

Loeb NG, Doelling DR, Wang HL, Su WY, Nguyen C, Corbett JG, Liang LS, Mitrescu C, Rose FG, Kato S (2018b) Clouds and the earth's radiant energy system (ceres) energy balanced and filled (ebaf) top-of-atmosphere (toa) edition-4.0 data product. J Clim 31(2):895–918. https://doi.org/10.1175/Jcli-D-17-0208.1

Loeb NG, Johnson GC, Thorsen TJ, Lyman JM, Rose FG, Kato S (2021c) Satellite and ocean data reveal marked increase in earth's heating rate. Geophys Res Lett 48(13):e2021GL093047. https://doi.org/10.1029/2021GL093047

Loeb NG, Mayer M, Kato S, Fasullo JT, Zuo H, Senan R, Lyman JM, Johnson GC, Balmaseda M (2022a) Evaluating twenty-year trends in earth's energy flows from observations and reanalyses. J Geophys Res-Atmos 127(12):e036686. https://doi.org/10.1029/2022JD036686

Morcrette JJ (2002) Assessment of the ecmwf model cloudiness and surface radiation fields at the arm sgp site. Mon Weather Rev 130(2):257–277

Paynter D, Ramaswamy V (2012) Variations in water vapor continuum radiative transfer with atmospheric conditions. J Geophys Res Atmos 117:D16310. https://doi.org/10.1029/2012jd017504

Paynter D, Ramaswamy V (2014) Investigating the impact of the shortwave water vapor continuum upon climate simulations using gfdl global models. J Gerontol Ser A Biol Med Sci 119(18):10720–10737. https://doi.org/10.1002/2014jd021881

Paynter DJ, Ramaswamy V (2011) An assessment of recent water vapor continuum measurements upon longwave and shortwave radiative transfer. J Geophys Res Atmos 116:D20302. https://doi.org/10.1029/2010jd015505

Pendergrass AG (2020) The global-mean precipitation response to co-induced warming in cmip6 models. Geophys Res Lett 47(17):e2020GL089964. https://doi.org/10.1029/2020GL089964

Pincus R, Mlawer EJ, Oreopoulos L, Ackerman AS, Baek S, Brath M, Buehler SA, Cady-Pereira KE, Cole JNS, Dufresne JL, Kelley M, Li JN, Manners J, Paynter DJ, Roehrig R, Sekiguchi M, Schwarzkopf DM (2015) Radiative flux and forcing parameterization error in aerosol-free clear skies. Geophys Res Lett 42(13):5485–5492. https://doi.org/10.1002/2015gl064291

Poli P, Hersbach H, Dee DP, Berrisford P, Simmons AJ, Vitart F, Laloyaux P, Tan DGH, Peubey C, Thépaut JN, Trémolet Y, Hólm EV, Bonavita M, Isaksen L, Fisher M (2016) Era-20c: An atmospheric reanalysis of the twentieth century. J Clim 29(11):4083–4097. https://doi.org/10.1175/Jcli-D-15-0556.1

Radel G, Shine KP, Ptashnik IV (2015) Global radiative and climate effect of the water vapour continuum at visible and near-infrared wavelengths. Q J R Meteorol Soc 141(688):727–738. https://doi.org/10.1002/qj.2385

Rienecker MM, Suarez MJ, Gelaro R, Todling R, Bacmeister J, Liu E, Bosilovich MG, Schubert SD, Takacs L, Kim GK, Bloom S, Chen JY, Collins D, Conaty A, Da Silva A, Gu W, Joiner J, Koster RD, Lucchesi R, Molod A, Owens T, Pawson S, Pegion P, Redder CR, Reichle R, Robertson FR, Ruddick AG, Sienkiewicz M, Woollen J (2011) Merra: Nasa's modern-era retrospective analysis for research and applications. J Clim 24(14):3624–3648. https://doi.org/10.1175/Jcli-D-11-00015.1

Roberts JB, Robertson FR, Clayson CA, Bosilovich MG (2012) Characterization of turbulent latent and sensible heat flux exchange between the atmosphere and ocean in merra. J Clim 25(3):821–838. https://doi.org/10.1175/Jcli-D-11-00029.1

Schmidt GA, Andrews T, Bauer SE, Durack PJ, Loeb NG, Ramaswamy V, Arnold NP, Bosilovich MG, Cole J, Horowitz LW, Johnson GC, Lyman JM, Medeiros B, Michibata T, Olonscheck D, Paynter D, Raghuraman SP, Schulz M, Takasuka D, Tallapragada V, Taylor PC, Ziehn T (2023) Ceresmip:

a climate modeling protocol to investigate recent trends in the earth's energy imbalance. Front Clim 5:1298599. https://doi.org/10.3389/fclim.2023.1298599

Slivinski LC, Compo GP, Whitaker JS, Sardeshmukh PD, Giese BS, McColl C, Allan R, Yin XG, Vose R, Titchner H, Kennedy J, Spencer LJ, Ashcroft L, Bronnimann S, Brunet M, Camuffo D, Cornes R, Cram TA, Crouthamel R, Dominguez-Castro F, Freeman JE, Gergis J, Hawkins E, Jones PD, Jourdain S, Kaplan A, Kubota H, Le Blancq F, Lee TC, Lorrey A, Luterbacher J, Maugeri M, Mock CJ, Moore GWK, Przybylak R, Pudmenzky C, Reason C, Slonosky VC, Smith CA, Tinz B, Trewin B, Valente MA, Wang XL, Wilkinson C, Wood K, Wyszynski P (2019) Towards a more reliable historical reanalysis: Improvements for version 3 of the twentieth century reanalysis system. Q J R Meteorol Soc 145(724):2876–2908. https://doi.org/10.1002/qj.3598

Stamatis M, Hatzianastassiou N, Korras-Carraca MB, Matsoukas C, Wild M, Vardavas I (2022b) Interdecadal changes of the merra-2 incoming surface solar radiation (ssr) and evaluation against geba & bsrn stations. Appl Sci-Basel 12(19):10176. https://doi.org/10.3390/app121910176

Stephens GL, Li JL, Wild M, Clayson CA, Loeb N, Kato S, L'Ecuyer T, Stackhouse PW, Lebsock M, Andrews T (2012) An update on earth's energy balance in light of the latest global observations. Nat Geosci 5(10):691–696. https://doi.org/10.1038/Ngeo1580

Takacs LL, Suárez MJ, Todling R (2016) Maintaining atmospheric mass and water balance in reanalyses. Q J R Meteorol Soc 142(697):1565–1573. https://doi.org/10.1002/qj.2763

Trenberth KE, Fasullo JT, Kiehl J (2009) Earth's global energy budget. Bull Am Meteor Soc 90(3):311. https://doi.org/10.1175/2008bams2634.1

Trenberth KE, Solomon A (1994) The global heat-balance - heat transports in the atmosphere and ocean. Clim Dyn 10(3):107–134. https://doi.org/10.1007/s003820050039

von Schuckmann K, Minière A, Gues F, Cuesta-Valero FJ, Kirchengast G, Adusumilli S, Straneo F, Ablain M, Allan RP, Barker PM, Beltrami H, Blazquez A, Boyer T, Cheng LJ, Church J, Desbruyeres D, Dolman H, Domingues CM, García-García A, Giglio D, Gilson JE, Gorfer M, Haimberger L, Hakuba MZ, Hendricks S, Hosoda S, Johnson GC, Killick R, King B, Kolodziejczyk N, Korosov A, Krinner G, Kuusela M, Landerer FW, Langer M, Lavergne T, Lawrence I, Li YH, Lyman J, Marti F, Marzeion B, Mayer M, MacDougall AH, McDougall T, Monselesan DP, Nitzbon J, Otosaka I, Peng J, Purkey S, Roemmich D, Sato K, Sato K, Savita A, Schweiger A, Shepherd A, Seneviratne SI, Simons L, Slater DA, Slater T, Steiner AK, Suga T, Szekely T, Thiery W, Timmermans ML, Vanderkelen I, Wjiffels SE, Wu TH, Zemp M (2023) Heat stored in the earth system 1960–2020: Where does the energy go? Earth Syst Sci Data 15(4):1675–1709. https://doi.org/10.5194/essd-15-1675-2023

von Schuckmann K, Palmer MD, Trenberth KE, Cazenave A, Chambers D, Champollion N, Hansen J, Josey SA, Loeb N, Mathieu PP, Meyssignac B, Wild M (2016) An imperative to monitor earth's energy imbalance. Nat Clim Change 6(2):138–144. https://doi.org/10.1038/Nclimate2876

Wang QY, Zhang H, Yang S, Chen Q, Zhou XX, Xie B, Wang YY, Shi GY, Wild M (2022) An assessment of land energy balance over east asia from multiple lines of evidence and the roles of the tibet plateau, aerosols, and clouds. Atmos Chem Phys 22(24):15867–15886. https://doi.org/10.5194/acp-22-15867-2022

Wild M (2008) Short-wave and long-wave surface radiation budgets in gcms: a review based on the ipcc-ar4/cmip3 models. Tellus A 60(5):932–945. https://doi.org/10.1111/J.1600-0870.2008.00342.X

Wild M (2017) Towards global estimates of the surface energy budget. Curr Clim Change Rep 3(1):87–97. https://doi.org/10.1007/s40641-017-0058-x

Wild M (2020) The global energy balance as represented in cmip6 climate models. Clim Dyn 55(3–4):553–577. https://doi.org/10.1007/s00382-020-05282-7

Wild M, Folini D, Hakuba MZ, Schar C, Seneviratne SI, Kato S, Rutan D, Ammann C, Wood EF, Konig-Langlo G (2015) The energy balance over land and oceans: an assessment based on direct observations and cmip5 climate models. Clim Dyn 44(11–12):3393–3429. https://doi.org/10.1007/s00382-014-2430-z

Wild M, Folini D, Schar C, Loeb N, Dutton EG, Konig-Langlo G (2013) The global energy balance from a surface perspective. Clim Dyn 40(11–12):3107–3134. https://doi.org/10.1007/s00382-012-1569-8

Wild M, Hakuba MZ, Folini D, Dörig-Ott P, Schär C, Kato S, Long CN (2019) The cloud-free global energy balance and inferred cloud radiative effects: an assessment based on direct observations and climate models. Clim Dyn 52:4787–4812. https://doi.org/10.1007/s00382-018-4413-y

Wild M, Ohmura A, Gilgen H, Morcrette JJ, Slingo A (2001) Evaluation of downward longwave radiation in general circulation models. J Clim 14(15):3227–3239. https://doi.org/10.1175/1520-0442(2001)014%3c3227:Eodlri%3e2.0.Co;2

Wild M, Ohmura A, Gilgen H, Roeckner E (1995) Validation of general-circulation model radiative fluxes using surface observations. J Clim 8(5):1309–1324

Wild M, Ohmura A, Gilgen H, Roeckner E, Giorgetta M, Morcrette JJ (1998) The disposition of radiative energy in the global climate system: Gcm-calculated versus observational estimates. Clim Dyn 14(12):853–869

Yu LS (2019) Global air-sea fluxes of heat, fresh water, and momentum: Energy budget closure and unanswered questions. Annu Rev Mar Sci 11:227–248. https://doi.org/10.1146/annurev-marine-010816-060704